Impact of low-dose radiation on nitrided lateral 4H-SiC MOSFETs and the related mechanisms

Wen-Hao Zhang(张文浩)[1,†], Ma-Guang Zhu(朱马光)[2,†], Kang-Hua Yu(余康华)[3], Cheng-Zhan Li(李诚瞻)[4], Jun Wang(王俊)[3], Li Xiang(向立)[1], and Yu-Wei Wang(王雨薇)[3,‡]

[1] *College of Materials Science and Engineering, Hunan University, Changsha* 410082, *China*
[2] *School of Integrated Circuits, Nanjing University, Suzhou* 210008, *China*
[3] *College of Electrical and Information Engineering, Hunan University, Changsha* 410082, *China*
[4] *State Key Laboratory of Advanced Power Semiconductor Devices, Zhuzhou CRRC Times Semiconductor Co., Ltd., Zhuzhou* 412001, *China*

(Received 30 November 2022; revised manuscript received 3 February 2023; accepted manuscript online 20 February 2023)

Lateral type n-channel 4H-SiC metal–oxide–semiconductor field effect transistors (MOSFETs), fabricated using a current industrial process, are irradiated with gamma rays at different irradiation doses in this paper to carry out a profound study on the generation mechanism of radiation-induced interface traps and oxide trapped charges. Electrical parameters (e.g., threshold voltage, subthreshold swing and channel mobility) of the device before and after irradiation are investigated, and the influence of the channel orientation ($[1\bar{1}00]$ and $[11\bar{2}0]$) on the radiation effect is discussed for the first time. A positive threshold voltage shift is observed at very low irradiation doses ($<$ 100 krad (Si)); the threshold voltage then shifts negatively as the dose increases. It is found that the dependence of interface trap generation on the radiation dose is not the same for doses below and above 100 krad. For irradiation doses $<$ 100 krad, the radiation-induced interface traps with relatively high generation speeds dominate the competition with radiation-induced oxide trapped charges, contributing to the positive threshold voltage shift correspondingly. All these results provide additional insight into the radiation-induced charge trapping mechanism in the SiO_2/SiC interface.

Keywords: SiC MOSFET, gamma-ray irradiation, interface traps, oxide-trapped charges

PACS: 73.20.–r, 73.40.Qv, 61.80.Az, 85.30.–z **DOI:** 10.1088/1674-1056/acbd2e

1. Introduction

Silicon carbide (SiC) is an attractive wide band gap semiconductor material with a relatively high breakdown field, thermal conductivity, and electron saturation velocity, especially when compared with its silicon (Si) counterparts. Due to these superior properties, the SiC metal–oxide–semiconductor field effect transistor (MOSFET) has become a desirable device in the field of high-power, high-temperature and fast-switching applications.[1] Additionally, the wide band gap and strong covalent bond of the material bring about inherent radiation tolerance, further providing the SiC device with great application potential in new-generation spacecraft.[2]

In recent years, several groups have studied the total ionizing dose (TID) response of 4H-SiC MOSFETs and experimentally observed that the electrical characteristics of the devices usually exhibit a negative threshold voltage shift after irradiation.[3–6] Just like Si MOSFETs, numerous studies link the electrical characteristic changes of the devices before and after irradiation to the radiation-induced interface traps and oxide traps.[7–10] Meanwhile, since 4H-SiC MOSFETs have long suffered from poor interface quality,[11–13] nitric oxide (NO) or nitrous oxide (N_2O) post-annealing has been utilized in the production of commercial 4H-SiC MOSFETs to suppress the interface trap density.[14–16] However, many studies suggest that interface nitridation not only passivates the intrinsic defects but also introduces additional interface and/or near-interface oxide traps as well,[17] making the trapping mechanism in 4H-SiC MOSFETs more complex and significantly different from that of Si MOSFETs. Therefore, it is necessary to thoroughly discuss the influence of the complex properties of the SiC interface on its irradiation characteristics. Additionally, previous works mainly focused on the radiation effect under a relatively high radiation dose (typically $>$ 300 krad).[9,18,19] However, according to bias-temperature instability research, interface traps tend to have a significant impact on the electrical characteristics of the 4H-SiC MOSFETs, especially in the early stage of operation.[20] Thus, the effect of charge trapping at low doses may be non-negligible, which also needs to be intensively investigated.

In this work, the effect of γ-ray radiation on lateral n-channel 4H-SiC MOSFETs, fabricated using a current industrial process, are studied. Electrical parameters, such as the shift of the threshold voltage, subthreshold swing and field effect mobility, under different radiation doses are extracted and discussed. Particularly, the influence of the channel orientation ($[1\bar{1}00]$ and $[11\bar{2}0]$) on the radiation effect for the 4H-SiC MOSFET is investigated for the first time. Furthermore, we find that the threshold voltage of the radiated device first shifts

[†]These authors contributed equally to this work.
[‡]Corresponding author. E-mail: yuweiwang@hnu.edu.cn

© 2023 Chinese Physical Society and IOP Publishing Ltd

toward the positive voltage side (< 100 krad) and then to the negative side (> 100 krad), which was not observed in previous reports. Also, the corresponding generation mechanism of radiation-induced interface traps and oxide trapped charges is discussed in detail in Section 3.

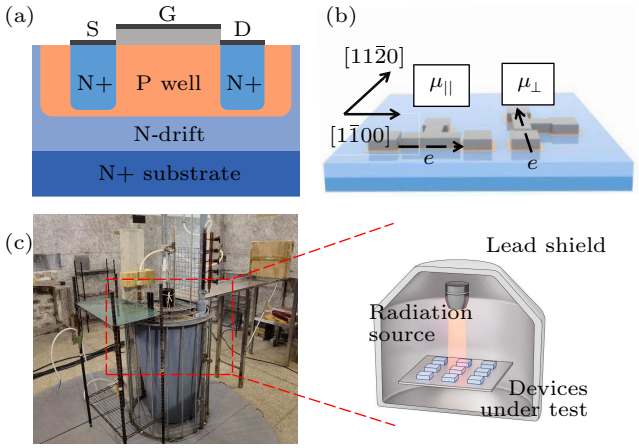


Fig. 1. The main parameters of the lateral MOSFET.

2. Experimental details

2.1. Devices under test

In this work, the lateral n-channel SiC MOSFETs are fabricated on an n-type 4H-SiC epilayer, which is grown on a standard SiC (0001) wafer with a 4° off-axis toward [11$\bar{2}$0]. The cross-section of the device is schematically shown in Fig. 1(a). The P well and the N+ source region are formed by heavy dose aluminum and nitrogen ion implantation, sequentially. Then, gate oxide is thermally grown in dry oxygen, followed by nitric oxide annealing. The main parameters of the devices are listed in Table 1. Notably, we fabricated the lateral 4H-SiC MOSFET along two perpendicular crystal orientations ([1$\bar{1}$00] and [11$\bar{2}$0]), as illustrated in Fig. 1(b); thus the influence of the crystal orientation on the total ionization dose response of the 4H-SiC MOSFET can be investigated. Figure 1(c) shows the radiation experimental setup, where the devices under test are placed in a lead shield to receive radiation from the radiation source.

Table 1. Main parameters of the lateral MOSFET.

Parameter	Value
Channel length	500 μm
Channel width	88 μm
Oxide thickness	57 nm
N+ doping	1×10^{19} cm^{-3}
N− doping	8×10^{15} cm^{-3}
P well doping	1.5×10^{17} cm^{-3}

2.2. Radiation experiment and electrical measurement

The SiC MOSFET devices are irradiated with a cobalt-60 (^{60}Co) γ-ray source at a dose rate of approximately 560 rad (Si)/s at room temperature. Zero biases are applied to the gate electrodes, and the source and drain electrodes are grounded during irradiation. The drain current–drain voltage curves (I_d–V_d curves) and drain current–gate voltage curves (I_d–V_g curves) of the devices are measured before and after the radiation, using a semiconductor characterization system (Keithley, 4200-SCS) at room temperature. The time interval between radiation and electrical characterization is controlled within 30 min to reduce the under-estimation of threshold voltage (V_{th}) shift caused by recovery.

3. Results and discussion

3.1. Unirradiated SiC MOSFETs

Figures 2(a) and 2(b) show the I_d–V_d curves at V_g of 5 V, 10 V, 15 V, 20 V, and 25 V for two unirradiated devices with channels along the [1$\bar{1}$00] and [11$\bar{2}$0] directions, respectively. The directions along [1$\bar{1}$00] and [11$\bar{2}$0] separately represent channel directions parallel or perpendicular to the surface steps on the (0001) SiC wafer due to step-flow growth.[21] Notably, the anisotropy of SiC devices is due to different microstructure characteristics of the channel and has been reported previously.[22,23] In this work, the I_d–V_d curves of the two devices also show a minor deviation, with the I_d of device [1$\bar{1}$00] being a little larger than that of [11$\bar{2}$0]. In Fig. 2, the I_d at $V_g = 25$ V and $V_d = 2$ V is 2.77 μA and 2.74 μA for the [1$\bar{1}$00] and [11$\bar{2}$0] directions, respectively.

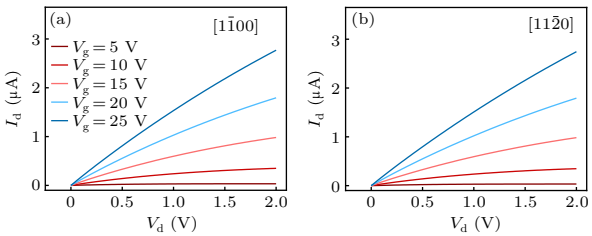


Fig. 2. The I_d–V_d curves at different gate voltages for unirradiated devices with channels along (a) [1$\bar{1}$00] and (b) [11$\bar{2}$0] directions.

3.2. Radiation results

To experimentally investigate the effect of γ-ray radiation on lateral n-channel 4H-SiC MOSFETs, the output and transfer characteristics before and after irradiation are demonstrated in Fig. 3. The pre-and-post irradiation I_d–V_d curves at $V_g = 25$ V for devices with channels along the [1$\bar{1}$00] and [11$\bar{2}$0] directions are shown in Figs. 3(a) and 3(b), respectively. The postirradiation curves are measured at six different radiation doses, with an accumulated total dose of 20 krad, 50 krad, 80 krad, 100 krad, 200 krad, and 300 krad (Si). As we can clearly see from Figs. 3(a) and 3(b), the I_d–V_d curves for devices with channels along the [1$\bar{1}$00] and [11$\bar{2}$0] directions both show a slight increase in I_d as the irradiation dose ramps up, and quantitative analysis and mechanism discussion will be shown later. Figures 3(c) and 3(d) show the to-

tal dose dependent I_d–V_g curves for the devices at $V_d = 0.2$ V. The I_d–V_g curves first shift negatively at doses of 20 krad and 50 krad. Then, an abnormal positive shift of the I_d–V_g curve is observed for both $[1\bar{1}00]$ and $[11\bar{2}0]$ devices when the total dose is 80 krad and 100 krad (see the light blue curves in the inset), which is rarely reported by previous works and the mechanism will be discussed later. With the radiation dose rising to above 100 krad, the I_d–V_g curves then show a negative shift, which increases with the dose as expected.

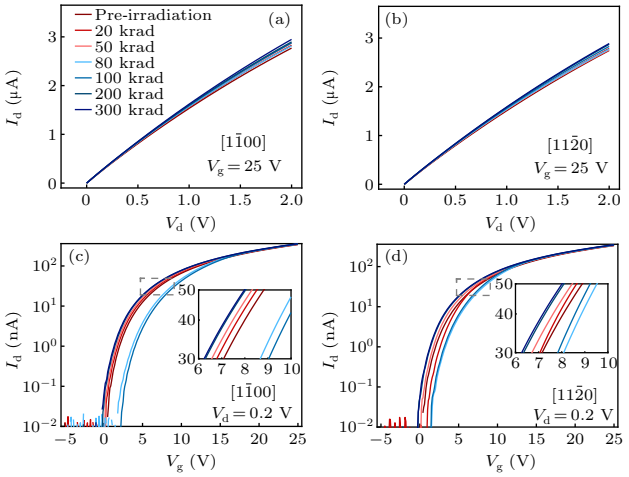


Fig. 3. The I_d–V_d curves at different total doses for devices with channels along (a) $[1\bar{1}00]$ and (b) $[11\bar{2}0]$ direction; I_d–V_g curves at different total doses for devices with channels along (c) $[1\bar{1}00]$ and (d) $[11\bar{2}0]$ direction.

To better analyze the irradiation response of the devices, electrical parameters as a function of the total doses are extracted from Fig. 3 and depicted in Fig. 4. It can be seen clearly in Fig. 4(a) that the I_{on} at $V_g = 25$ V and $V_d = 2$ V increases slightly with irradiation doses in the overall trend, but demonstrates an anomalous trough at total doses of 50 krad–80 krad. We also extracted the subthreshold swing (SS), which represents the amount of V_g needed to modulate I_d by a decade. It is obtained at a logarithmic coordinate from the subthreshold region (corresponding to I_d of 1×10^{-10} A–1×10^{-8} A in this paper) and given by $SS = \partial V_g / \partial \log I_d$. As shown in Fig. 4(b), the SS of the I_d–V_g curves at $V_d = 0.2$ V has a small fluctuation in the range of 1.7 V/dec–2.1 V/dec. There is also an obvious rise at the dose of 80 krad, particularly for the device along the $[1\bar{1}00]$ direction. According to previous reports, the change in SS represents the degree of degradation of the device, and the dependency of the change in the interface trap density (D_{it}) on the SS can be described by the following expression:[24]

$$\Delta D_{it} = \frac{C_{ox}}{\ln(10)\, qkT}(SS_{after} - SS_{before}), \tag{1}$$

where C_{ox} is the capacitance of the gate oxide, q is the electronic charge, k is the Boltzmann constant and T is the absolute temperature. Accordingly, the significant rise in the value of SS at 80 krad represents the increase in interface traps, which is accordant with the results in Fig. 4(a) in that considerable electrons in the channel are trapped and I_{on} is decreased correspondingly.

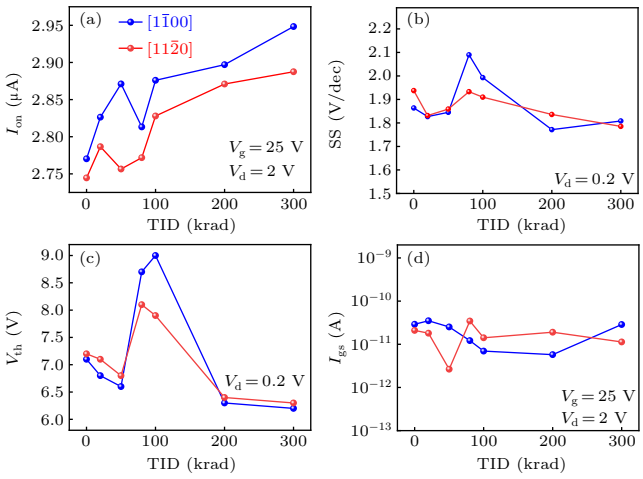


Fig. 4. Total dose dependent (a) I_{on}; (b) SS; (c) V_{th}; (d) I_{gs} extracted from curves in Fig. 3, for the devices with channels along $[1\bar{1}00]$ and $[11\bar{2}0]$ direction separately.

Furthermore, as shown in Fig. 4(c), we analyze the threshold voltage (V_{th}, determined as the V_g at $I_d = 30$ nA) of the irradiated devices in Fig. 3. When the total doses are 0 krad, 20 krad, 50 krad, 80 krad, 100 krad, 200 krad, and 300 krad, the corresponding V_{th} are 7.1 V, 6.8 V, 6.6 V, 8.7 V, 9 V, 6.3 V, and 6.2 V in device $[1\bar{1}00]$ and 7.2 V, 7.1 V, 6.8 V, 8.1 V, 7.9 V, 6.4 V, and 6.3 V in device $[11\bar{2}0]$, respectively. A significant positive shift of V_{th} is observed at total doses < 100 krad. When the dose is increased to above 100 krad, the V_{th} then decreases with the dose, like other published reports.[25,26] We attribute the large fluctuation of V_{th} at low-dose irradiation (< 100 krad) to the intense competitive relationship between radiation-induced oxide trapped charges and radiation-induced interface traps, and the corresponding trapping mechanism will be discussed in Subsection 3.4. To our knowledge, little work has observed positive V_{th} shifts of SiC MOSFETs after irradiation; we think it is probably because the previous works mainly focus on the radiation effect under a relatively high γ-ray radiation dose (typically > 300 krad)[9,19] due to the strong radiation tolerance of SiC. Additionally, it is worth mentioning that we have tested other devices (fabricated with the same structure and processing method) under similar irradiation conditions. A positive V_{th} shift at low doses is also observed, demonstrating that this phenomenon is not caused by accidental measurement error.

In the gate-source leakage current (I_{gs}), no obvious change is observed in the I_d–V_g curves in Fig. 3. And we can see it more clearly in Fig. 4(d), where the I_{gs} for the irradiated devices at $V_g = 25$ V and $V_d = 2$ V remain essentially unchanged at the $\sim 10^{-11}$ A level, suggesting that the irradiation up to 300 krad does not significantly degrade the insulation characteristics of the gate oxide.

3.3. Electrical characteristic anisotropy

Although the anisotropy of 4H-SiC has been reported,[27,28] the dependency of the radiation effect of 4H-SiC MOSFETs on the crystal orientation has not been discussed yet. As we can see clearly from Figs. 4(a)–4(d), the lateral 4H-SiC MOSFET devices show obvious anisotropy in the irradiation response. The electrical characteristics of the device with the channel along the $[1\bar{1}00]$ crystal orientation demonstrate greater changes after irradiation than those of the $[11\bar{2}0]$ device under the same test conditions.

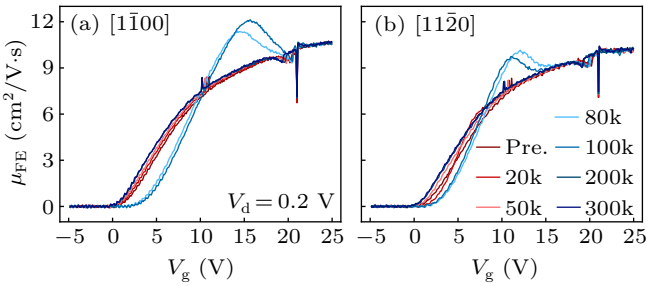


Fig. 5. The μ_{FE} curves at different total doses for devices with channels along (a) $[1\bar{1}00]$ and (b) $[11\bar{2}0]$ direction separately.

Furthermore, we extract the field effect mobility (μ_{FE}) from the transfer characteristics in Figs. 3(a) and 3(b), using the following relation:[29]

$$\mu_{FE} = \frac{g_m L}{W C_{ox} V_d}, \tag{2}$$

where g_m is the transconductance taken at a linear coordinate, L and W are the channel length and width, and C_{ox} is the gate capacitance per unit of area. As Figs. 5(a) and 5(b) show, the μ_{FE} for both device $[1\bar{1}00]$ and device $[11\bar{2}0]$ change only slightly after 300 krad exposure, but show obvious abnormal peaks at 80 krad and 100 krad. We suspect the deviation of μ_{FE}–V_g curves is relevant to the radiation-induced interface traps discussed in the previous section; the generation of abnormal peaks at 80 krad and 100 krad and the increase in total mobility may be the result of a change in the complex competition pattern among Coulomb scattering, phonon scattering and surface roughness scattering, which need further investigation. The μ_{FE} of irradiated 4H-SiC MOSFETs also demonstrates anisotropy. The peak value for the $[1\bar{1}00]$ sample is higher than that for the $[11\bar{2}0]$ sample, particularly at 80 krad or 100 krad. As previously mentioned in Subsection 3.1, the channel orientation of the $[1\bar{1}00]$ sample is parallel to the surface steps, while that of the $[11\bar{2}0]$ sample is perpendicular to the steps, typically with higher interface roughness and effective defect density.[22,30] It is believed that this is caused by the incomplete crystal planes at the interface, which favor the generation of disordered atomic regions and increase the density of dangling bonds.[23] Thus, we believe that the anisotropic transport properties of the irradiated devices are essentially caused by different microstructure characteristics of the interface, and quantitative research needs to be carried out in the future.

3.4. Trapping mechanism discussion

It has been widely accepted that the physical processes (see Fig. 6) leading from the initial deposition of energy by ionizing radiation to the creation of radiation-induced defects include: (i) generation of electron–hole pairs (EHPs); (ii) prompt recombination of a fraction of EHPs and fast escape of electrons; and (iii) transport of holes remaining in oxide, either generation of oxide trapped charges or interface traps.[31–34] Essentially, for the n-channel MOSFET, the shift of V_{th} towards either the negative or positive voltage side can be interpreted in terms of the competition of generation numbers between radiation-induced oxide trapped charges and acceptor-like interface traps. The traditional model assumes the number of radiation-induced interface traps is much less than that of radiation-induced oxide trapped charges, so that the influence of interface traps can be almost ignored, which has well explained the negative shift of V_{th} for irradiated SiC MOSFETs in previous studies.[9] However, as Fig. 4(c) shows, V_{th} shifts positively at doses $<$ 100 krad and then negatively at doses $>$ 100 krad, indicating the above trapping mechanism assumption is no longer valid in our test conditions.

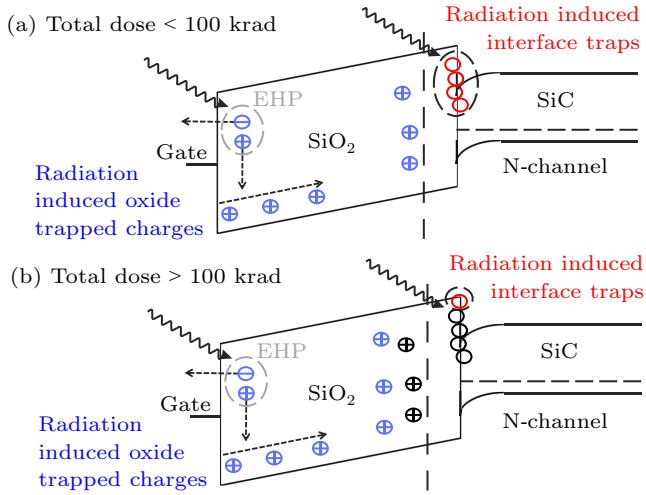


Fig. 6. Schematic of radiation-induced oxide trapped charge and interface trap mechanism at (a) total doses $<$ 100 krad and (b) total doses $>$ 100 krad. The black pattern indicates the previously increased oxide trapped charges and interface traps at total doses $<$ 100 krad.

Based on the experimental results, we speculate that the defect generation at doses below and above 100 krad follows different rules, as schematically illustrated in Fig. 6. For radiation doses $<$ 100 krad, considerable oxide trapped charges and acceptor-like interface traps are generated during radiation via hole trapping by bulk defects and interface reactions through precursors, respectively. The generation number of interface traps (negatively charged) is estimated to be relatively high, which is comparable with that of oxide trapped charges

(positively charged), resulting in the shift of $V_{\rm th}$ between positive and negative, as shown in Fig. 4(c). Although the production mechanism of radiation-induced interface traps in SiC MOS has not yet been fully revealed, it can be mentioned that rapid generation of the interface traps at low doses has also been observed in a TID study on nitrided capacitors.[35] Based on the existing studies, it is speculated that the rapid generation of interface traps at low doses may be associated with the depassivation of carbon-related defects, and the exact mechanism needs to be further investigated.[35,36] With regard to radiation doses $>$ 100 krad, the trapping mechanism is consistent with the published studies. The radiation-induced oxide trapped charges absolutely dominate the competition with radiation-induced interface traps and increase with the increasing radiation dose, resulting in a continuous negative shift of $V_{\rm th}$ correspondingly. To our knowledge, positive shifts in $V_{\rm th}$ after radiation have rarely been reported for SiC MOSFETs, which we attribute to the fact that previous works mainly focus on the radiation effect under a relatively high radiation dose ($>$ 300 krad) due to the high $[1\bar{1}00]$ radiation tolerance of SiC. Thus, the contribution of radiation-induced interface traps in the early total dose range ($<$ 100 krad) is significantly ignored or underestimated and deserves further investigation.

3.5. Analysis of interface traps and oxide trapped charges

To conduct a quantitative analysis of the trapping mechanism of our irradiated SiC MOSFET, the charge separation technique developed by McWhorter and Winokur is used to draw the generation numbers of the radiation-induced oxide trapped charges and interface traps.[10,37] According to the technique, the threshold voltage shift ($\Delta V_{\rm th}$) can be expressed as

$$\Delta V_{\rm th} = \Delta V_{\rm it} + \Delta V_{\rm ot}, \tag{3}$$

where $\Delta V_{\rm it}$ is the voltage shift caused by interface trapped charges, and $\Delta V_{\rm ot}$ is the voltage shift caused by oxide trapped charges. The charge separation technique considers the interface traps to be approximately neutral when the Fermi energy level overlaps with the midgap and the threshold voltage shift is only affected by the oxide trapped charges.[9] Therefore, $\Delta V_{\rm ot}$ is regarded as the shift of the midgap voltage ($V_{\rm mg}$), which is the corresponding $V_{\rm g}$ in the $I_{\rm d}$–$V_{\rm g}$ curve when $I_{\rm d} = I_{\rm mg}$. The midgap current ($I_{\rm mg}$) is extracted using the following equation:

$$I_{\rm mg} = \frac{W\mu_{\rm n}}{L\beta^2}\sqrt{\frac{q\varepsilon_{\rm s}N_{\rm A}}{2\varphi_{\rm s}}}\left(\frac{n_{\rm i}}{N_{\rm A}}\right)^2\left(1-{\rm e}^{-\beta V_{\rm d}}\right){\rm e}^{\beta\varphi_{\rm s}}, \tag{4}$$

where $\mu_{\rm n}$ is the electron mobility, $\varphi_{\rm s}$ is the surface potential, $N_{\rm A}$ is the channel doping, $n_{\rm i}$ is the intrinsic carrier concentration, and $\beta = q/kT$. Then, $\Delta V_{\rm it}$ can be calculated by Eq. (3). The dependency of the corresponding $\Delta V_{\rm ot}$ and $\Delta V_{\rm it}$ on the radiation dose for device $[1\bar{1}00]$ is illustrated in Fig. 7(a). During the radiation, $\Delta V_{\rm ot}$ showed an overall decreasing trend, while $\Delta V_{\rm it}$ showed an obvious trend of first increasing and then decreasing. The density variations of oxide trapped charges ($\Delta N_{\rm ot}$) and interface trapped charges ($\Delta N_{\rm it}$) are then calculated by

$$\Delta N_{\rm it} = \frac{C_{\rm ox}}{q}\Delta V_{\rm it}, \tag{5}$$

$$\Delta N_{\rm ot} = \frac{C_{\rm ox}}{q}\Delta V_{\rm ot}, \tag{6}$$

where $C_{\rm ox}$ is the capacitance of oxide per unit area, and q is the absolute value of unit electronic charge. The calculated $\Delta N_{\rm it}$ and $\Delta N_{\rm ot}$ during irradiation for device $[1\bar{1}00]$ are depicted in Fig. 7(b). The density of interface trapped charges increases rapidly and peaks at low radiation doses ($<$ 100 krad), then drops abruptly after 100 krad and begins to increase slowly, which is basically consistent with the previous trend of SS in Fig. 4(b). This change in $\Delta N_{\rm it}$ was also observed in the study by Dixit *et al.*[35], and was particularly significant for the capacitors after nitridation. The density of oxide trapped charges remains increased overall, just like other previously published works. The difference is that, as a result of the combined effect of the two types of trapped charges, the $V_{\rm th}$ of the devices exhibit a positive shift at a low radiation dose and a negative shift at a high radiation dose. It is worth mentioning that at 80 krad and 100 krad, the density of the generated interface trapped charges is significantly higher than the generated oxide trapped charges, thus demonstrating that the positive shift of the threshold voltage is caused by interface trapped charges.

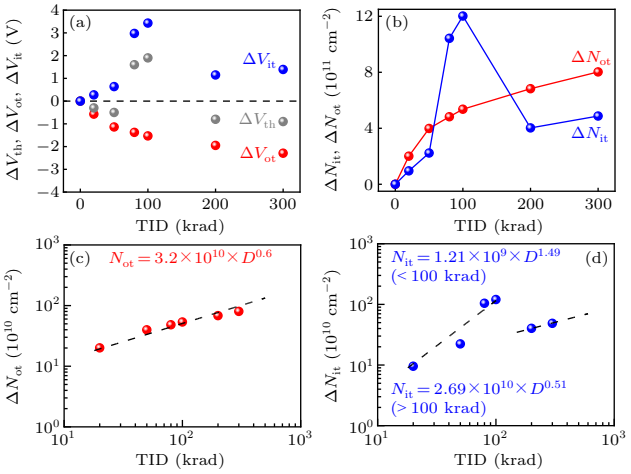


Fig. 7. Total dose dependent (a) voltage shifts; (b) changes in oxide trapped charge and interface trapped charge; (c) changes in oxide trapped charge and simulated changes in its density; (d) changes in interface trapped charge and simulated changes in its density in device $[1\bar{1}00]$.

To evaluate the quantitative changes in the two types of trapped charges and predict their trends, we use the power-law TID model proposed by Petrosjanc *et al.*,[38] where $\Delta N_{\rm it}$ and $\Delta N_{\rm ot}$ can be fitted by the following formula:

$$\Delta N_{\rm it} = A_{\rm it} \times D^{B_{\rm it}}, \tag{7}$$

$$\Delta N_{\rm ot} = A_{\rm ot} \times D^{B_{\rm ot}}. \tag{8}$$

The fitting curves are represented by dashed lines in Figs. 7(c) and 7(d), where ΔN_{it} is fitted in segments with a cut-off point of 100 krad. The exponential $B_{ot} = 0.6$ obtained from ΔN_{ot} is essentially the same as the typical ones.[1] Comparatively, the power-law TID exponent obtained from ΔN_{it} at low doses ($B_{it} = 1.49$) is much higher than the typical value in previous literature ($B_{it} = 0.67$[1,7]). As a consequence, although the number of oxide trapped charges is larger than that of interface traps and leads to a negative shift of V_{th} at 20 krad and 50 krad, the interface traps already outnumber the oxide trapped charges and lead to a positive shift of V_{th} at 80 krad and 100 krad. However, the power-law TID exponent at high doses is substantially lower ($B_{it} = 0.51$). It can be predicted that at higher doses, the density of oxide trapped charges will be much higher than the density of interface trapped charges, resulting in a continuous negative shift of the threshold voltage. This corroborates the previous inference that, due to the different mechanisms of radiation-induced generation of interface traps at different radiation doses, the factor that mainly affects the shift of V_{th} changes from interface trapped charges to oxide trapped charges with increasing radiation dose. Additionally, we also analyzed the trapped charge variation of device $[11\bar{2}0]$ (not shown here), and the interface traps also demonstrate high and low generation rates at low and high doses respectively, which further validates our proposed new mechanism as being universally applicable.

4. Conclusion

This paper discusses the TID response mechanism of lateral type n-channel 4H-SiC MOSFETs, fabricated using current industrial processes. The electrical parameters of the devices show different degrees of shift under various radiation doses, and the anisotropy of the radiation effect with respect to the channel orientation is investigated for the first time. The mobility before and after irradiation of device $[1\bar{1}00]$ with the channel parallel to the steps on the epilayer is higher and more variable than that of device $[11\bar{2}0]$ with the channel perpendicular to the steps, which is essentially caused by the higher interface roughness and effective defect density at the perpendicular intersection of the channel and the step.

In addition, we found that the shift of the threshold voltage after irradiation was related to a competitive relationship between radiation-induced oxide trapped charges and radiation-induced interface traps. For irradiation doses $<$ 100 krad, the radiation-induced interface traps have a relatively high generation speed and thus dominate the competition with radiation-induced oxide trapped charges. But for irradiation doses $>$ 100 krad, the density of radiation-induced interface traps decreases while the radiation-induced oxide trapped charges keep increasing, suggesting a different mechanism than for radiation doses $<$ 100 krad. Since we investigated the mechanism of threshold voltage shift at a low irradiation dose for the first time, it can be considered as an important reference basis for conducting subsequent irradiation studies in the future. All these results provide a better understanding of the radiation-induced charge trapping mechanism in the SiO_2/SiC interface.

Acknowledgments

Project supported by the National Natural Science Foundation of China (Grant Nos. 52107190 and 62101181) and China Postdoctoral Science Foundation (Grant No. 2021M700203).

References

[1] Yoshikawa M, Itoh H, Morita Y, Nashiyama I, Misawa S, Okumura H and Yoshida S 1991 *J. App. Phys.* **70** 1309
[2] Li H J, Zhang Y M, Tang X Y, Li D X and Song Q W 2018 *1st Workshop on Wide Bandgap Power Devices and Applications in Asia*, May 16–18, 2018, Xi'an, China, p. 156
[3] Ahyi A C, Wang S R and Williams J R 2006 *Mater. Sci. Forum.* **527–529** 1063
[4] Mitomo S, Matsuda T, Murata K, Yokoseki T, Makino T, Takeyama A, Onoda S, Ohshima T, Okubo S, Tanaka Y, Kandori M, Yoshie T and Hijikata Y 2017 *Phys. Status Solidi A* **214** 1600425
[5] Yu Q K, Waqas A, Cao S, Wang H, Lv H, Sun Yi, Mo R, Wang Q Y, Mei B, Sun J J, Zhang H W, Tang M, Bai S, Zhang T, Bai Y and Zhang C R 2022 *IEEE Trans. Nucl. Sci.* **69** 1127
[6] Sun Y B, Wan X, Liu Z Y, Jin H, Yan J Z, Li X J and Shi Y L 2022 *Radiat. Phys. Chem.* **197** 110219
[7] Ohshima T, Yoshikawa M, Itoh H, Aoki Y and Nashiyama I 1998 *Jpn. J. Appl. Phys.* **37** L1002
[8] Fleetwood D M 2020 *IEEE Trans. Nucl. Sci.* **67** 1216
[9] Hu D Q, Zhang J W, Jia Y P, Wu Y, Peng L and Tang Y 2018 *IEEE Trans. Electron Devices* **65** 3719
[10] Winokur P S, Schwank J R, McWhorter P J, Dressendorfer P V and Turpin D C 1984 *IEEE Trans. Nucl. Sci.* **31** 1453
[11] Kimoto T, Kaneko M, Tachiki K, Ito K, Ishikawa R, Chi X, Stefanakis D, Kobayashi T and Tanaka H 2021 *IEEE International Electron Devices Meeting*, December 11–16, 2021, San Francisco, CA, USA, p. 36.1.1
[12] Cabello M, Soler V, Rius G, Montserrat J, Rebollo J and Godignon P 2018 *Mater. Sci. Semiconductor Process.* **78** 22
[13] Pande P, Haasmann D, Han J, Moghadam H A, Tanner P and Dimitrijev S 2020 *Microelectron. Rel.* **112** 113790
[14] Wang M H, Yang M C, Liu W H, Qi J W, Yang S Q, Han C Y, Geng L and Hao Y 2021 *IEEE Trans. Electron Devices* **68** 1841
[15] Luo Z P, Wan C P, Jin Z and Xu H Y 2021 *Semicond. Sci. Tech.* **36** 045021
[16] Jia Y F, Lv H L, Tang X Y, Han C, Song Q W, Zhang Y M, Zhang Y M, Dimitrijev S, Han J S and Haasmann D 2019 *Mater. Electron.* **30** 10302
[17] Okamoto D, Yano H, Oshiro Y, Hatayama T, Uraoka Y and Fuyuki T 2009 *Appl. Phys. Exp.* **2** 021201
[18] Ohshima T, Yokoseki T, Murata K, Matsuda T, Mitomo S, Abe H, Makino T, Onoda S, Hijikata Y, Tanaka Y, Kandori M, Okubo S and Yoshie T 2016 *Jpn. J. Appl. Phys.* **55** 01AD01
[19] Takeyama A, Makino T, Okubo S, Tanaka Y, Yoshie T, Hijikata Y and Ohshima T 2019 *Materials* **12** 2741
[20] Zhang E X, Zhang C X, Fleetwood D M, Schrimpf R D, Dhar S, Ryu S H, Shen X and Pantelides S T 2012 *IEEE Trans. Device Mater. Rel.* **12** 391
[21] Via F L, Camarda M and Magna A L 2014 *Appl. Phys. Rev.* **1** 031301
[22] Scharnholz S, Stein von Kamienski E, Gölz A, Leonhard C and Kurz H 1998 *Mater. Sci. Forum.* **264–268** 1001
[23] Woerle J, Johnson B, Bongiorno C, Yamasue K, Ferro G, Dutta D, Jung T, Sigg H, Cho Y, Grossner U and Camarda M 2019 *Phys. Rev. Mater.* **3** 084602

[24] Schroder D K 2005 *Semiconductor Material and Device Characterization* (3rd ed) (Hoboken: Wiley) p. 360
[25] Murata K, Mitomo S, Matsuda T, Yokoseki T, Makino T, Onoda S, Takeyama A, Ohshima T, Okubo S, Tanaka Y, Kandori M, Yoshie T and Hijikata Y 2017 *Phys. Status Solidi A* **214** 1600446
[26] Akturk A, McGarrity J M, Potbhare S and Goldsman N 2012 *IEEE Trans. Nucl. Sci.* **59** 3258
[27] Hjelm M, Bertilsson K and Nilsson H E 2001 *Appl. Surf. Sci.* **184** 194
[28] Saks N S, Ancona M G and Lipkin L A 2004 *Mater. Sci. Forum*. **457–460** 689
[29] Fiorenza P, Giannazzo F, Frazzetto A and Roccaforte F 2012 *J. Appl. Phys.* **112** 084501
[30] Lee K K, Ohshima T, Ohi A, Itoh H and Pensl G 2006 *Jpn. J. Appl. Phys.* **45** 6830
[31] Barnaby H J 2006 *IEEE Trans. Nucl. Sci.* **53** 3103
[32] Zhu M G, Xiao H S, Yan G P, Sun P K, Jiang J H, Cui Z, Zhao J W, Zhang Z Y and Peng L M 2020 *Nat. Electron.* **3** 622
[33] Zhu M G, Zhou J S, Sun P K, Peng L M and Zhang Z Y 2021 *ACS Appl. Mater. Interfaces* **13** 47756
[34] Wang X, Zhu M G, Li X Q, Qin Z Z, Lu G H, Zhao J W and Zhang Z Y 2022 *Adv. Mater.* **34** 2204066
[35] Dixit S K, Dhar S, Rozen J, Wang S, Schrimpf R D, Fleetwood D M, Pantelides S T, Williams J R and Feldman L C 2006 *IEEE Trans. Nucl. Sci.* **53** 3687
[36] Knežević T, Hadžipašić A, Ohshima T, Makino T and Capan I 2022 *Appl. Phys. Lett.* **120** 252101
[37] McWhorter P J and Winokur P S 1986 *Appl. Phys. Lett.* **48** 133
[38] Petrosjanc K O and Kharitonov I A 1993 *Proceedings of IEEE International Conference on Microelectronic Test Structures*, March 22–25, 1993, Sitges, Spain, p. 9